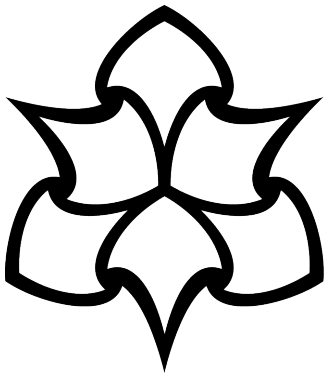

A 23-28 GHz pHEMT MMIC Low-Noise Amplifier for Satellite-Cellular Convergence Applications

Mfonobong Uko[1] and Sunday Ekpo[2]

Abstract – *Satellite-cellular convergence promises to enable higher millimetre-wave bandwidth (data rate); beamformed better signal alignment (higher system efficiency); multi-connectivity (higher data rates); and new use cases (verticals). Harnessing these opportunities will depend on overcoming challenges spanning shorter distance/reduced coverage and component complexity; construction of antenna array and over-the-air testing; coexistence issues between multiple mobile communication connections; performance tests; cybersecurity. This paper presents a broadband monolithic microwave integrated circuit (MMIC) low-noise amplifier (LNA) based on a 0.15 µm gate length Gallium Arsenide (GaAs) pseudomorphic high electron transistor (pHEMT) technology for satellite-cellular convergence use cases applications. The designed three-stage 23-28 GHz LNA demonstrates an industry-leading flat gain response of 30 dB, a noise figure of 1.70 dB and a very low power dissipation of 43 mW. The differential sensitivity response spans 0.01 µs to 0.04 dBm/Hz over the upper and lower ends of the channel bandwidths of the 5G New Release frequency range n258 band (24.25-27.58 GHz). Moreover, the millimetre-wave regenerative sensitivity analysis of the designed LNA holds a grand promise for real-time component-level reconfiguration applications. These applications include dynamic spectrum access; regenerative wireless transponder-transceiver technologies support; active spectrum resource usage; distributed sensing over a multi-standards wideband spectrum; and massive and complex time-varying spectrum datasets/features.*

Keywords: *Amplifier; Gain; K/Ka-Band; Low Noise; Noise Figure; Satellite; Transceiver.*

Nomenclature

3G	Third-generation
4G	Fourth-generation
5G	Fifth-generation
BER	Bit error ratio
CNR	Carrier-to-noise ratio
ENP	Effective noise power
ETRI	Electronics and telecommunications research institute
f_d	Resonant frequency
FISCA	Fibre-integrated satellite communication architecture
f_{max}	Maximum oscillation frequency
f_T	Gain frequency
GaAs	Gallium arsenide
LNA	Low-noise amplifier
LNB	Low-noise block
LO	Local oscillator
MDS	Minimum detectable signal
MER	Modulation error ratio
MMIC	Monolithic microwave integrated circuit
NF	Noise figure
pHEMT	Pseudomorphic high electron transistor
PLL	Phase-locked loop
P_r	Received power
RATs	Radio access technologies
RoF	Radio-over-fiber
SNR	Signal-to-noise ratio
UE	User equipment
VCO	Voltage-controlled oscillator
V_{ds}	Drain-source voltage
V_{gs}	Gate-source voltage

I. Introduction

The role communication satellites play today, from 'connecting the unconnected' to providing secure and seamless device-to-device communications, cannot be overemphasised. Space communication architectures, therefore, are going to play a vital role in the 5G ecosystem [1], taking advantage of the proposed 5G wider coverage, higher throughput and lower latency [2], [3], while incorporating existing 3G and 4G technologies to provide faster connections [4], [5]. One prerequisite for

5G is to permit a similar network for anybody, anyplace, whenever and this is the aspect the satellite [6] is expected to complement any terrestrial infrastructure deployed.

The massive scale connections involving sensors networked throughout the entire production system will provide remote real-time and non-real-time monitoring, ensuring ubiquitous seamless process operations continuity. Multi-protocol communication and pan-cloud computing (including industrial IoTs, big data, artificial intelligence and 5G) can improve product development efficiency and enable previously impractical manufacturing functions. However, integrating an advanced connectivity technology requires an informed examination of adaptable network bandwidth; long-haul remote coverage, system security; and critical and non-critical remote manufacturing plant resources monitoring. Satellite-enabled 5G internet of things sensors will constitute a significant game-changer for the integrated commercial and industrial sector [7]. Satellite-enabled backhaul for big data analytics, ultra-reliable low-latency connectivity, and massive scale computing nodes will create a safer, intelligent, and efficient future manufacturing system. Hence, there is a need to characterise the user terminals performance metrics (including transmit power, receive sensitivity, operating frequency, and long- and short-haul links) of satellite-enabled 5G internet of things sensors profiling for industry 4.0 applications. The receiver front-end sensitivity modelling scope will span integrated connectivity for the edge, gateway, and enterprise nodes within the industry 4.0 hierarchy.

Like previous generations, 5G will use various frequency bands ranging from the Sub-1 GHz, 1-6 GHz and above 6 GHz bands. The European Union has designated the 24.25 - 27.5 GHz band as a pioneer 5G band. This millimetre-wave spectrum offers very high data capacity and speeds with vast communication resources. MmWave 5G networks are also becoming prominent for service providers, as consumer demands for data overshadow the sub-6 GHz networks [7]. Several satellite-enabled services are already key ingredients in existing terrestrial networks (2G, 3G, and 4G).

With the 5G standard(s) evolution, the existing networks are incorporated into the emerging 5G ecosystem to meet the horizontal and vertical application's needs (Fig. 1). Figure 1a shows four use cases for satellite integration with the 5G network. The satellite is used to access areas difficult to reach, complement the existing terrestrial backhaul for broadband services, connect with users on the move as applicable in aeroplanes and ships, and provide direct assistance to under-served areas. Figure 1b shows the integration alongside the 5G access network to alleviate the throughput burden from the terrestrial backhaul.

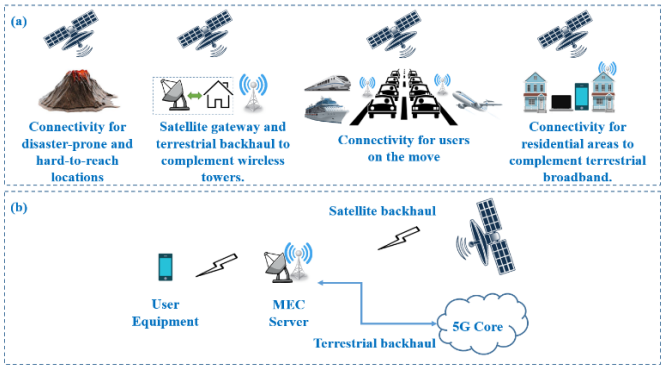

Fig. 1. Satellite Network Integration for 5G. (a) Satellite Use case deployment with 5G network architecture. (b) Satellite complementary integration with 5G access network.

The proposed integrated Satellite-Cellular Convergence systems must deliver high mobile broadband and reliable transmission of high-speed data from the transmitter front-end to the receiver front-end. This requires a critical analysis of the satellite link performance [8], taking into consideration large-capacity communication, the noise level, power level and sensitivity of the overall satellite system, to cope with various communication demands of space and terrestrial applications [9] - [11].

The low noise amplifier is a vital building block of the receiver front-end of the satellite transponder subsystem. It determines the system's overall noise performance and reliability in terms of the satellite link performance [8]. Traditionally, the LNA is matched to 50 Ω input and output sources. The LNA should be designed to obtain the lowest possible noise for the satellite and 5G application receivers. If its performance falls short, the entire receiver circuity and system performance will be degraded for the designed satellite and 5G communication applications.

In this paper, a 0.15 µm pseudomorphic high electron mobility transistor (pHEMT) process is used to design an LNA for integrated satellite and 5G communication applications. The LNA is created using a 3-stage common source configuration based on industry standards and exhibits a low noise figure. Section II presents the assigned frequencies for the 5G connectivity ecosystem use cases. Section III reviews various active device technology and a suitable design process for our design. The broadband design procedures for an MMIC LNA are presented in Section IV. Section V presents the achieved results with their interpretation. Section VI concludes the paper.

II. 5G Frequency Bands Assignment

With the 5G standards out, mm-wave frequency bands are proposed as the best candidates to satisfy the insatiable demand for high data rate, speed and bandwidth by consumers. The 5G wireless evolution brings cutting-edge technology to enable a higher than 10 Gbps download

speed using the vast millimetre-wave (mm-Wave) spectrum. As a result, millimetre-wave satellite hardware development for space and terrestrial 5G communications is inevitable for seamless transmission of data between the transmitter and receiver front-ends and complimenting existing terrestrial networks to deliver coverage to hard-to-reach areas. The third-generation partnership project (3GPP) specifies two fundamental frequency ranges (FR) for 5G communication applications. Since the cm-/mm-wave spectrum exhibit different behaviours, the radio frequency (RF) specifications requirements for FR1 and FR2 are defined separately in many cases (Table I).

TABLE I
5G SPECIFICATIONS FREQUENCY

Frequency Range	Range covered in Rel. 15 (MHz)
FR1	450 - 6000
FR2	24250 - 52600

The 5G ecosystem deployment in the millimetre-wave region is very fractal due to its unpredictable behaviour above 20 GHz. The framework is proficient given a line-of-sight scenario but highly unstable for non-line of sight. Furthermore, the high attenuation through obstacles, foliage, raindrops reduces the signal power level, hence a significant challenge along the propagation path. Deployment of phased arrays partially deals with this limitation, hence the need for a robust and efficient low noise amplifier design, sensitive enough to detect and amplifier the attenuated signal received to reduce the path loss in the propagation path.

In this paper, a 23 - 28 GHz monolithic microwave integrated circuit (MMIC) low-noise amplifier is designed using the pseudomorphic high electron mobility transistor (pHEMT) process technology for the 5G New Release (NR) FR2. This frequency range covers both 5G and satellite communications applications [12] [13], [14]. To analyse the proposed 5G receiver sensitivity, the NR channel bandwidth for FR2 (Table II) is utilised. The critical advanced radio access technology (RAT) implementation considerations for the 5G NR FR2 are higher in device development, measurement challenges, and new testing approaches. The millimetre-wave considerations include high bandwidth for high data rate; minimal high contiguous bandwidth at lower frequencies; high free-space path loss at high frequencies; and line-of-sight requirements.

TABLE II
NR CHANNEL BANDWIDTH FOR FR2

NR Band	SCS (kHz)	Channel Bandwidth (MHz)			
		50	100	200	400
n257	60	Yes	Yes	Yes	
	120	Yes	Yes	Yes	Yes
n258	60	Yes	Yes	Yes	
	120	Yes	Yes	Yes	Yes
n260	60	Yes	Yes	Yes	
	120	Yes	Yes	Yes	Yes
n261	60	Yes	Yes	Yes	
	120	Yes	Yes	Yes	Yes

The sub-carriers spacings (SCSs) are 60 kHz and 120 kHz for all the channel bandwidths except the 400 MHz channel (which supports only the 120 SCS). The MMIC LNA is designed to cover the proposed new NR bands in FR2 (Table III).

TABLE III
NEW NR BANDS IN FR2

Band Number	Uplink (GHz)	Downlink (GHz)	Bandwidth (MHz)	Duplex Mode
n257	26.5-29.5	26.5-29.5	3000	TDD
n258	24.25-27.58	24.25-27.58	3250	TDD
n260	37-40	37-40	3000	TDD
n261	27.5-28.35	27.5-28.35	850	TDD

III. Active Device Technology Selection

Next-generation wireless systems are aimed at millimetre-wave frequencies, and selecting the proper process technology is vital based on the required operational specification of the intended application. For a successful design to be achieved, a combination of active (diode, transistors) and passive (inductor, capacitors) devices must be selected, using a well-defined process technology to meet the design goals and expected level of performance of the system.

Active and passive elements are critical in the device technology selection due to the high losses at mmWave frequencies. Substrate losses and quality factor of matching networks are also significant in the active device selection, as transmission line insertion loss improves with higher resistivity substrates.

Next-generation 5G satellite receivers must meet the criteria of providing high sensitivity and selectivity over broad bandwidths, covering existing communication standards and 5G systems between 24 GHz to 40 GHz, named as n257, n258, n260 and n261(Table III). To achieve this, the receiver front-end LNA, being the most critical block, should be designed and optimised to give high gain and linearity over the required frequency band. This high gain and linearity are a function of choosing suitable transistor technologies such as the gallium-arsenide (GaAs) pseudomorphic high-electron-mobility transistors (pHEMTs) and silicon-germanium (SiGe) heterojunction bipolar transistors (HBTs).

The pHEMT process technology offers a high power-added efficiency performance with excellent low noise. It generally fits applications in which optimisation of the

receiver front-end sensitivity is essential, thus its broad use in satellite, radar, and microwave radio systems. The LNA is designed using a 0.15 µm InGaAs pHEMT process that demonstrates outstanding noise performance, lower cost and better robustness at microwave frequencies [15]. The device has a cut-off frequency (f_T) of 110 GHz and a maximum oscillation frequency (f_{max}) of higher than 150 GHz. The chosen design process foundry includes Metal-Insulator-Metal (MIM) capacitors, spiral inductors, backside VIA holes and thin-film resistors used in the design.

DC and RF test/measurements over different bias conditions are made to determine the transistor's operating point. This test determines an appropriate operating point for the required LNA, considering design requirements (especially the overall noise performance and dissipated power). The operating point chosen has a drain-source voltage (V_{ds}) = 2 V, gate-source voltage (V_{gs}) = -0.3 V and drain-source current (I_{ds}) = 0.021 A. The pHEMT active device (transistor) is biased for optimum low-noise performance for the K/Ka-band LNA. The characteristics curve for the transconductance of GaAs pHEMT is plotted. This determines the current through the output (drain) of the transistor to the voltage across the input (gate) of the transistor. Mathematically, the transconductance, g_{ms}, is:

$$g_m = \frac{\Delta I_{ds}}{\Delta V_{gs}} \qquad (1)$$

The transconductance value obtained is 81 mS at V_{ds} = 2 V; V_{gs} = -0.3 V; and I_{ds} = 0.021 A.

For a pHEMT device, the load reflection coefficient, Γ_{opt}, brings about a mismatch for a maximum power transfer condition, much different from the input return loss's conjugate reflection coefficient, S_{11}. However, with the suitable active device (transistor) selection, the Γ_{opt} and input return loss, S_{11} can be made much closer in value, resulting in a better output-power while still achieving low noise.

IV. Broadband MMIC Low Noise Amplifier Design.

A single-ended LNA is designed over the frequency range of 23-28 GHz for 5G communication applications. The active device makes use of a scalable PL15-10 0.15 µm low noise GaAs pseudomorphic high electron mobility transistor process technology provided. The LNA forms part of the RF receiver front-end in a transceiver, alongside the down-conversion mixer. Figure.2 shows a simplified receiver front-end with the LNA designed to have the reconfigurable capability for applications within the 23 - 28 GHz band. A feedback matrix is incorporated to select various frequencies required for communication devices. The reconfigurable impedance matching (*IM)* network can generate narrowband and wideband frequencies spanning f^1 to f^n. Each created band of interest (B) is based on the dynamic spectrum access for the channel-aware use case application. Mathematically, this feedback is given by:

$$\begin{bmatrix} IM^1{}_{f1} & \cdots & IM^1{}_{fn} \\ \vdots & \ddots & \vdots \\ IM^i{}_{f1} & \cdots & IM^i{}_{f1} \end{bmatrix} \begin{bmatrix} f^1 \\ \vdots \\ f^n \end{bmatrix} = \begin{bmatrix} B^1 \\ \vdots \\ B^i \end{bmatrix} \qquad (2)$$

The MMIC LNA is designed based on an inductive source-degenerated common-source configuration architecture biased for low-power consumption.

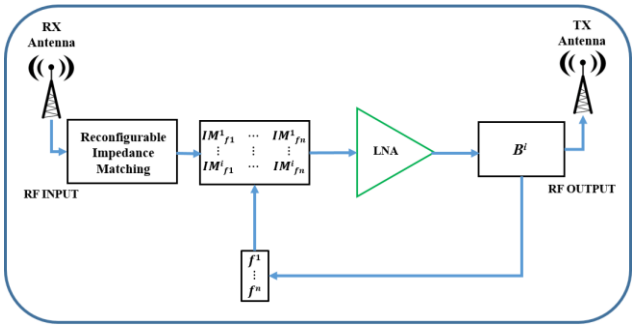

Fig. 2. A Proposed Reconfigurable RF Receiver Front-end subsystem (LNA) Architecture.

The most critical part of the amplifier design is the input matching network. The 50-Ω input termination is converted into a complex impedance close to the transistors' optimum noise match. A cascaded system is employed to achieve an appreciably high gain, noise performance, and negligible reflections at the input and output. This requires a judicious system tuning and optimisation to achieve the design goals for the LNA [16].

IV.1. Noise Characterisation

System noise performance is an essential figure-of-merit in microwave design that determines the overall signal integrity of the receiver front-end. For satellite systems (5G inclusive), the noise figure is determined using the performance matrices of the low noise amplifier, mixers, and oscillators.

For K/Ka-band satellite applications, the noise figure is critical in determining the overall system sensitivity; hence the first stage design of the LNA should be designed for low-noise capability. The noise equation in (3) further shows that the first stage's noise performance influences the overall noise performance of the LNA, hence optimum noise matching is necessary at the input.

$$F = F_1 + \frac{F_2 - 1}{G_{A1}} + \frac{F_3 - 1}{G_{A1}G_{A2}} + \cdots + \frac{F_n - 1}{G_{A1}G_{A2}\ldots G_{A(n-1)}} \qquad (3)$$

IV.2. K/Ka-Band LNA Design

The K/Ka-Band LNA design spans 23-28 GHz of the electromagnetic spectrum, covering the 24.25-27.5 GHz band earmarked for 5G. A cascade of three stages is chosen using PL15-10 0.15 µm low noise GaAs pseudomorphic high electron mobility transistor process technology. At millimetre-wave frequencies, the conventional single-stage amplifier exhibits relatively low gain and higher losses due to parasitic and passive effects. Increasing the number of stages to three (3) enhances the overall gain and noise suppression, even though this leads to an increase in the designed LNA's power consumption.

Table IV shows the MMIC LNA design consideration for each stage of the design, while Fig. 3 shows the design topology of the three-stage K/Ka-band LNA.

TABLE IV
MMIC DESIGN CONSIDERATION FOR THE THREE STAGES

Performance Metric	Stage 1	Stage 2	Stage 3
Goal(s)	Low noise and high gain	Stability, high gain.	Stability, Gain flatness and power.
Device size	2 x 50 µm	2 x 50 µm	4 x 50 µm
Stability	Source inductive feedback.	Source inductive feedback.	Source inductive feedback.
Matching Network	Optimum matching	Inter-stage matching	Maximum power transfer
Design transition	source impedance transformation to the optimum noise impedance	first stage transistor's output impedance transformation to the second stage transistor's input impedance	R-C parallel feedback for flat gain

For the LNA to meet the desired specification, the various design parameters (forward transmission gain, minimum noise figure, S-Parameter extraction, noise resistance, input and output isolations) were obtained at a bias gate-source voltage, V_{gs} = -0.3 V and drain-source voltage, V_{ds} = 2 V. The resonant frequency for this design, was f_d = 25 GHz. Spiral inductors and MIM capacitors are used for the matching networks to support the wideband operation requirement.

Fig. 4 shows the K/Ka-band LNA schematic, designed to achieve a low noise figure. The components descriptions and their role in the design is presented in Table V.

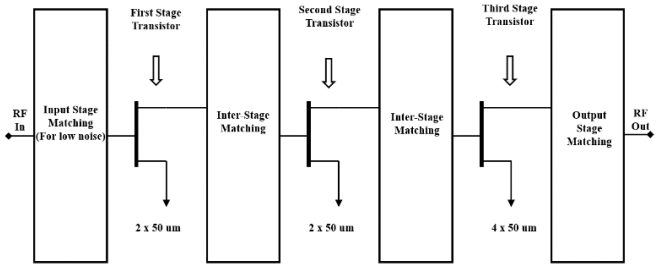

Fig. 3. Three-Stage K/Ka-Band LNA Topology

TABLE V
LNA COMPONENT PART LIST

Components	Decription	Function
C1 and C11	DC blocks	Preventing dc voltage from going through the RF path
C2, C4, C5, C7, C8 and C10	Decoupling capacitors	Short any RF signal from spilling into the voltage supply way
R1, R3, R5.	High resistive loads	Preventing RF leakage into the voltage supply path
C9 and R6	R-C network	Parallel feedback for flat gain
C1 and L1	L-C Network	Optimum noise input matching network
L6 and C11	L-C Network	Output matching network
TL1, TL2 and TL3	High impedance transmission lines	Source inductance for stability

IV.3. 5G NR FR2 Receiver Sensitivity Modelling

The LNA subsystem's performance metrics constitute the key design trade-offs in determining its sensitivity. This sensitivity shows the difference between the received power and the noise floor, defining the receiver's signal-to-noise ratio [13], [14]. Board- and device-levels variables optimisation are critical for subsystems performance enhancements [8]. This paper examines the relationship between the receiver's sensitivity and the noise floor over an NR FR2 band for satellite-cellular (5G) communication applications. The signal-to-noise ratio (SNR) in dB of a receiver is given by:

$$SNR = Pr - MDS \tag{4}$$

P_r = received power in dBm, and MDS = minimum detectable signal or receiver sensitivity in dBm.

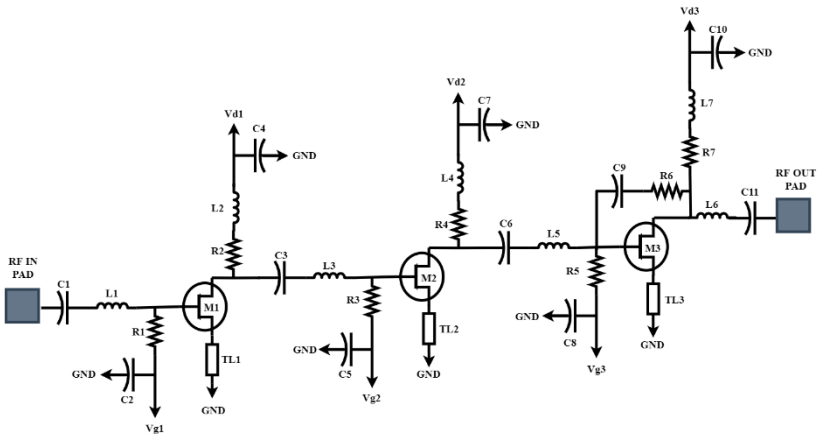

Fig. 4. A schematic of the designed K/Ka-Band LNA

The referenced receiver sensitivity estimating relationship, *S*, in dBm is given by:

$$S = 10(log10(KTB)) + NF + CNR \qquad (5)$$

where *K* is the Boltzmann's constant (= -228 dBW/(kHz); *T*, the thermodynamic temperature of the receiver in Kelvin; *B*, the channel bandwidth (resolution) of the signal; NF, the noise figure of the receiver in dB; and CNR, the carrier-to-noise ratio in dB. From equation (5), it is evident that a receiver's sensitivity depends on the bandwidth of all other parameters being within controllable boundaries. This is a result of the stringent operating conditions of the 5G NR FR2 receiver. Another critical challenge for receiver sensitivity is the need for spectral efficiency for the user equipment (UE) as the dynamic frequency translations of multi-band, multi-standards radio communication support massive machine-type high-speed systems. A differential deduction of the receiver sensitivity, based on the process technology of the front-end LNA subsystem responses, is proposed to mitigate these challenges. Hence, a reconfigurable front-end receiver (LNA) subsystem becomes inevitable as an ideal device architecture for satellite-cellular convergence use cases applications to achieve and sustain a constant in-band noise figure regime for multi-frequency advanced RAT network operations. Substituting equations (4) into (5), a receiver link model with thermal noise is derived as:

$$SNRr = \Pr(dBm) - (10(\log(10KTB)) + NF(dB) \quad (6)$$

V. Results and Discussion

The presented simulated MMIC LNA is designed using a scalable PL15-10 0.15 µm low noise GaAs pHEMT process technology. In the characterisation of MMIC LNAs, systematic and random errors are the two major concerns of the RF engineer. Hence, system calibration is an essential process that must be carried out to remove systematic errors. The most challenging systematic errors are directivity, source mismatch, reflection tracking, transmission line tracking, crosstalk and load mismatch. These measurement standards are obtained for the two ports of the device-under-test (DUT). On the other hand, random errors are uncontrollable changes that occur while the measurements are being carried out; they are stochastic and time-variant. The measurement calibration substrate configurations are short, open, load and through (SOLT) ports. Each is used to address a given systematic error. For example, the source mismatch and reflection tracking use the open and short calibration substrates, respectively. The 50-Ω load is used to calibrate for the directivity (finite isolation or amount of signal leakage) of the directional couplers. During an MMIC LNA characterisation, the allowable temperature drift is 23±1 ºC; some equipment allows for up to 3 ºC drift about the ambient temperature. For any given fabricated MMIC LNA that is characterised, 0.1 to 0.2 dB is the allowable loss margin for linear (S-parameters) measurements. A loss of above 1 dB is unacceptable. Losses also exist between the fabricated DUT and the simulated real components due to fabrication imperfections. Fabrication inconsistencies always affect the stability parameters of the DUT and cause it to oscillate. Hence, before its fabrication, designing an MMIC LNA with a very high stability factor (*k*) value is always recommended. This work utilised the real components of a commercial foundry library to achieve a first-pass design for a satellite-cellular convergence use case application.

V.1. K/Ka-Band LNA simulation analysis

The LNA input and output return losses are shown in Fig. 5. The output and input return losses responses are less than -10 dB for the entire band, showing the validity

of the amplifier's input and output matching networks for telecommunication applications. The effective gain (Fig. 6) is about 30 dB with a ripple factor of 1dB across the band of interest. The reverse gain (Fig. 7) is less than -40 dB (depicting good isolation) for the band of interest, while the minimum noise at the resonant frequency of 25 GHz is 1.7 dB (Fig. 8). The LNA is unconditionally stable across the entire band up to the cut-off frequency (Fig. 9). This good stability response proves to a good design unlikely to oscillate at any frequency. A summary of the designed LNA performances is given in Table VI. Fig. 10 is the gain versus input power plot showing the gain compression with an increase in the input power.

Fig. 11 shows the linearity of the LNA. The input P1dB corresponds to -22.3 dBm. Table VI summarises the results of the designed LNA at a centre-design frequency of 25 GHz.

TABLE VI
K/Ka-band LNA REQUIREMENTS AND PERFORMANCE AT 25 GHz DESIGN FREQUENCY

Design Parameter	Requirement	Performance
S_{11} (dB)	≤-10	-15
S_{12} (dB)	≤-40	-43
S_{21} (dB)	≥ 25	30
S_{22} (dB)	≤-10	-25
NF (dB)	<2	1.7
K (up to f_t @ 100 GHz)	>1	2
In-band Ripple (dB)	≤3	1

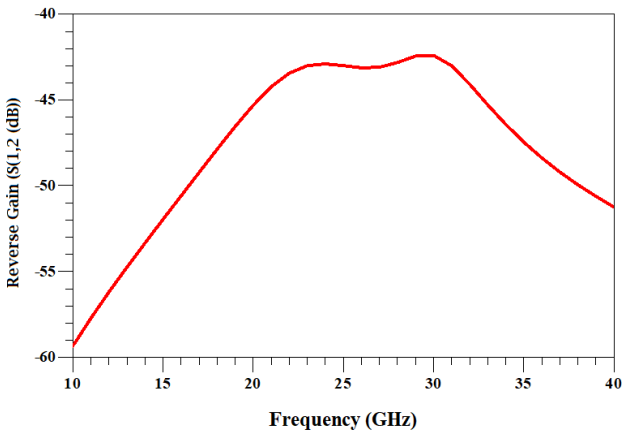

Fig. 7. Isolation of the K/Ka-band MMIC LNA circuit

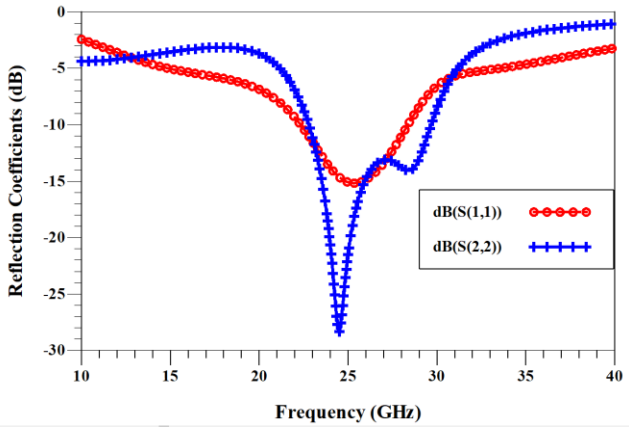

Fig. 5. Input and Output reflection coefficient of the K/Ka-band MMIC LNA circuit

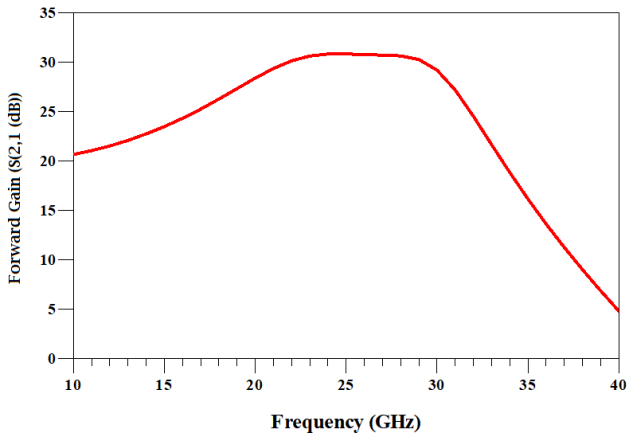

Figure 6. Gain of the K/Ka-band MMIC LNA circuit

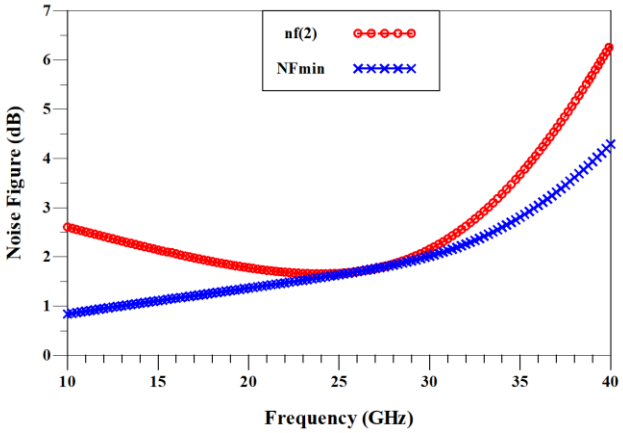

Fig. 8. Noise Figure of the K/Ka-band MMIC LNA circuit

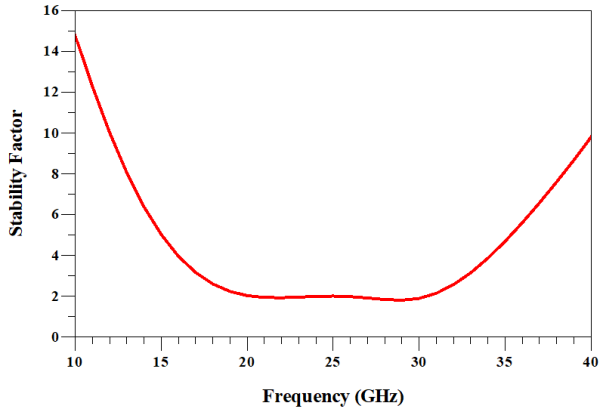

Fig. 9. Stability Factor of the K/Ka-band MMIC LNA circuit

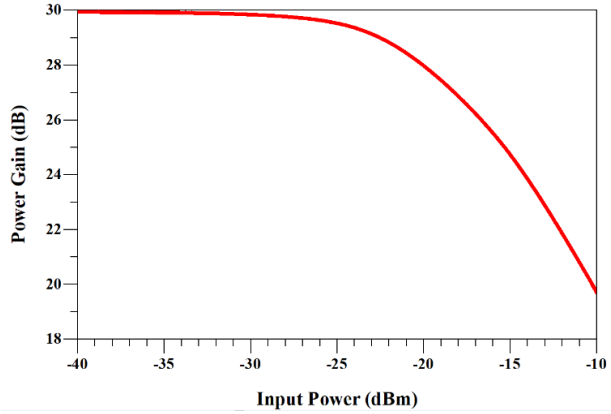

Fig. 10. Gain Vs Input Power Curve of designed K/Ka-band MMIC LNA

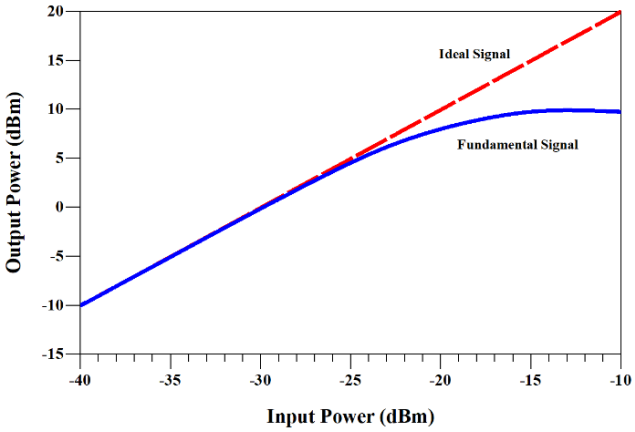

Fig. 11. Linearity curve of designed K/Ka-band MMIC LNA

V.2. 5G NR FR2 Receiver Sensitivity Simulation

To characterise and analyse the sensitivity response of the reported designed broadband 23-24 GHz pHEMT InGaAs MMIC LNA, a simulation of the performance metrics for a typical 5G NR FR2 receiver was carried out. The simulation parameters applied in (5) are shown in Table VII. The receiver's path loss constraints are considered for up to the industry-recommended 300 m range for 5G small cells.

TABLE VII
K/KA-BAND LNA SENSITIVITY SIMULATION PARAMETERS

Parameter	Value
Carrier-to-Noise Ratio	10 dB
NF	1.7 dB
5G NR FR2 band	n258

Fig. 12 shows the path-loss response for the 5G NR FR2 band n258 up to 300 m. The upper uplink and downlink bands of the proposed 5G Ka-band frequencies records at least 20 dB signal attenuation within a 300-m range. This finding implies a need to enhance the receiver sensitivity by performing a component to subsystem-level reconfiguration in near real-time.

Fig. 13 illustrates the 5G NR FR2 receiver sensitivity and noise floor responses over the proposed channel bandwidths of 50 MHz, 100 MHz, 200 MHz and 400 MHz. Our reported three-stage single-ended MMIC LNA design utilises the common-source configuration to achieve a flat gain and stability (up to the cut-off frequency of the active semiconductor device) with parallel feedback in stage three. In Fig. 14, a 5G NR FR2 receiver sensitivity differential response is presented. The response shows that the lower the 5G channel bandwidth, the steeper the pHEMT MMIC LNA device's sensitivity gradient. For the reported design, the 5G n258 band gradient over 50 MHz to 100 MHz is 0.04 dBm/Hz, while 200 MHz to 400 MHz yields 0.01 dBm/Hz. Hence, receiver sensitivity reduces with channel bandwidth, but narrowband resolutions imply considerable in-band sensitivity differential swings. This finding further strengthens the need for a reconfigurable receiver to cater for the massive 5G UE and base station transceivers operational requirements. Table VIII shows the comparison of the designed K/Ka-Band LNA with recently reported K/Ka-Band LNAs.

TABLE VIII
SIMULATION COMPARISON OF DESIGNED LNA AT K/Ka-band FREQUENCIES

Ref	Process	No. of Stages	Freq. (GHz)	Gain (dB)	Noise (dB)	Power (mW)
[11]	0.15 µm GaAs pHEMT	2 (MMIC)	30-38	17	2.6	100
[17]	28 nm CMOS	3 (MMIC)	20-27	26	4.78	131
[18]	22 nm FDSOI	2 (MMIC)	23-27	28.5	2.38	20
[19]	GaAs pHEMT	3 (MMIC)	18-21.6	30.3	1	60
[15]	0.4 µm CMOS	2 (MMIC)	24-39	12.9	3.9 – 4.9	15.5
[20]	0.13 µm SiGe	1 (MMIC)	28	16.2	2.8	8.2

[21]	HMC active device	2 (MMIC)	27-30	39	2.8	420
This Work	0.15 µm GaAs pHEMT	3 (MMIC)	23-28	30.8	1.7	43

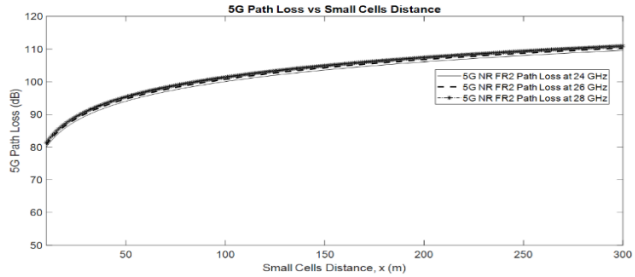

Fig. 12. 5G NR FR2 Path Loss versus Small Cells Distance

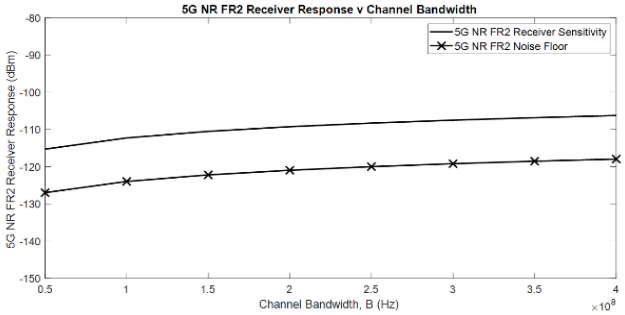

Fig. 13. 5G NR FR2 Receiver Sensitivity Response

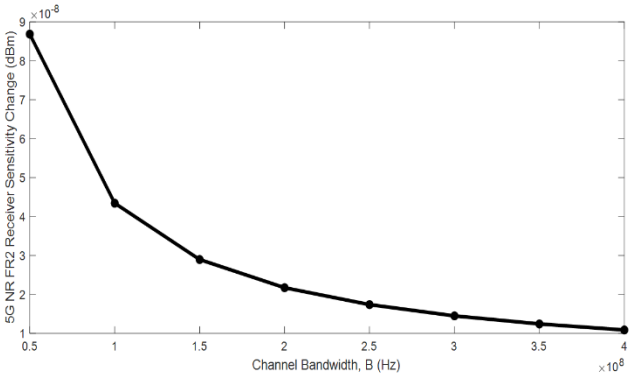

Fig. 14. 5G NR FR2 Receiver Sensitivity Differential Response

VI. Conclusion

Satellite-cellular convergence connectivity ecosystem promises a seamless, ubiquitous heterogeneous mix of higher bandwidth and data rate technologies spanning proximity, wireless personal area network, wireless local area network, wireless neighbourhood network, and wireless wide-area network. User and base station equipment complexity at the millimetre-wave frequency range is a non-trivial development challenge. A three-stage K/Ka-band MMIC LNA has been designed and reported in this paper. The pHEMT process technology was utilised, and the receiver front-end's performance metrics satisfy the telecommunications industry requirements for the 5G New Release frequency range n258 band for satellite-cellular convergence use cases applications. The average input and output reflection coefficients are better than -12 dB and -14 dB, respectively. The amplifier stability up to the cut-off frequency is greater than two and meets the fabrication defects standards for zero oscillation performance. The in-band ripple is 1 dB, and the average noise figure within the operating frequency band of interest is 1.74 dB. The 5G path loss constraints for a 300-m small cells architecture are accommodated by the reported wideband MMIC LNA performance responses. The sensitivity response to channel bandwidth variations is mainly bandwidth dependent. The reported research findings promise to reduce system integration and deployment complexity and user and base station equipment costs for satellite-cellular convergence use cases applications.

REFERENCES

1. M. Karavolos, N. Nomikos, D. Vouyioukas and P. T. Mathiopoulos, "HST-NNC: A Novel Hybrid Satellite-Terrestrial Communication With NOMA and Network Coding Systems," in IEEE Open Journal of the Communications Society, vol. 2, pp. 887-898, 2021.

2. Q. Huang, M. Lin, W. -P. Zhu, J. Cheng and M. -S. Alouini, "Uplink Massive Access in Mixed RF/FSO Satellite-Aerial-Terrestrial Networks," in IEEE Transactions on Communications, vol. 69, no. 4, pp. 2413-2426, April 2021.

3. Bai, L.; Zhu, L.; Zhang, X.; Zhang, W.; Yu, Q. Multi-Satellite Relay Transmission in 5G: Concepts, Techniques, and Challenges. IEEE Network 2018, 32, 38-44.

4. Nawaz, A.A.; Albrecht, J.D.; Cagri Ulusoy, A. A 28-/60-GHz Band-Switchable Bidirectional Amplifier for Reconfigurable mm-Wave Transceivers. *IEEE Transactions on Microwave Theory and Techniques 2020*, 68,3197-3205.

5. A. S. Youssouf, M. H. Habaebi and N. F. Hasbullah, "The Radiation Effect on Low Noise Amplifier Implemented in the Space-Aerial–Terrestrial Integrated 5G

Networks," in IEEE Access, vol. 9, pp. 46641-46651, 2021.

6. Y. Cho, H. -K. Kim, M. Nekovee and H. -S. Jo, "Coexistence of 5G With Satellite Services in the Millimeter-Wave Band," in IEEE Access, vol. 8, pp. 163618-163636, 2020.

7. M. Uko and S. Ekpo, "8-12 GHz pHEMT MMIC Low-Noise Amplifier for 5G and Fiber-Integrated Satellite Applications", *International Review of Aerospace Engineering (IREASE)*, vol. 13, no. 3, p. 99, 2020.

8. Ekpo, S.C.; George, D. Impact of Noise Figure on a Satellite Link Performance. IEEE Communications Letters 2011, 15, 977-979.

9. Kumar, A.R.A.; Dutta, A.; Sahoo, B.D. A Low-Power Reconfigurable Narrowband/Wideband LNA for Cognitive Radio-Wireless Sensor Network. IEEE Transactions on Very Large-Scale Integration (VLSI) Systems 2020,28,212-223.

10. I. Leyva-Mayorga et al., "LEO Small-Satellite Constellations for 5G and Beyond-5G Communications," in IEEE Access, vol. 8, pp. 184955-184964, 2020.

11. L. Yang, L. Yang, T. Rong, Y. Li, Z. Jin and Y. Hao, "Codesign of Ka-Band Integrated GaAs PIN Diodes Limiter and Low Noise Amplifier," in IEEE Access, vol. 7, pp. 88275-88281, 2019.

12. Lee, W.; Hong, S. 28 GHz RF Front-End Structure Using CG LNA as a Switch. IEEE Microwave and Wireless Components Letters 2020, 30, 94-97.

13. Ekpo, S. Parametric System Engineering Analysis of Capability-based Small Satellite Missions. IEEE Systems Journal 2019, 13, 110.

14. Ekpo, S.C. Thermal Subsystem Operational Times Analysis for Ubiquitous Small Satellites Relay in LEO. International Review of Aerospace Engineering (IREASE) 2018, 11, 48.

15. R. A. Shaheen, T. Rahkonen and A. "Millimeter-wave Frequency Reconfigurable Low Noise Amplifiers for 5G,". IEEE Transactions on Circuits and Systems II: Express Briefs 2021, 68, 642-646..

16. Ekpo, S.; Kharel, R.; Uko, M. A Broadband LNA Design in Common-Source Configuration for Reconfigurable Multi-standards Multi-bands Communications. 2018 ARMMS RF and Microwave Conference, 2018, pp. 1-10.

17. C. -J. Liang et al., "A K/Ka/V Triband Single-Signal-Path Receiver With Variable-Gain Low-Noise Amplifier and Constant-Gain Phase Shifter in 28-nm CMOS," in IEEE Transactions on Microwave Theory and Techniques 2021.

18. O. El-Aassar and G. M. Rebeiz, "Design of Low-Power Sub-2.4 dB Mean NF 5G LNAs Using Forward Body Bias in 22 nm FDSOI," in IEEE Transactions on Microwave Theory and Techniques, vol. 68, no. 10, pp. 4445-4454, Oct. 2020.

19. Cha, E.; Wadefalk, N.; Nilsson, P.; Schleeh, J.; Moschetti, G.; Pourkabirian, A.; Tuzi, S.; Grahn, J. 0.3-14 and 16-28 GHz Wide-Bandwidth Cryogenic MMIC Low-Noise Amplifiers. IEEE Transactions on Microwave Theory and Techniques 2018, 66, 4860-4869. doi:10.1109/TMTT.2018.2872566.

20. A. A. Nawaz, J. D. Albrecht and A. Çağrı Ulusoy, "A Ka/V Band-Switchable LNA With 2.8/3.4 dB Noise Figure," in IEEE Microwave and Wireless Components Letters, vol. 29, no. 10, pp. 662-664, Oct. 2019.

21. F. Alimenti et al., "A Ka-Band Receiver Front-End With Noise Injection Calibration Circuit for CubeSats Inter-Satellite Links," in IEEE Access, vol. 8, pp. 106785-106798, 2020.

Authors' information

Communication and Space Systems Engineering Team, Department of Engineering, Faculty of Science and Engineering, Manchester Metropolitan University, Manchester, M1 5GD, UK.
E-mails: [1]m.uko@mmu.ac.uk;
[2]scekpo@ieee.org; S.Ekpo@mmu.ac.uk;

Mfonobong Uko received his B.Eng. degree in Electrical/Electronic Engineering from the University of Uyo, Nigeria and MSc in Communication Engineering from The University of Manchester, UK. He is a PhD candidate in Communication Engineering at the Manchester Metropolitan University, UK. His research interest is adaptive satellite system design; multi-physics design, and modelling of RF, microwave, millimetre-wave, and optical transceivers; internet of things sensors characterisation; multi-objective system engineering; and complex systems optimisation.

Sunday C. Ekpo obtained the MSc. Degree in Communication Engineering from the University of Manchester, Manchester, UK in September 2008 and proceeded for his PhD degree in Electrical and Electronic Engineering at the same institution. He specialises in highly adaptive satellite system design; multi-physics design, and modelling of RF, microwave, millimetere-wave, and optical transceviers; internet of things sensors characterisations; multi-objective system engineering; and complex systems optimisation.

He holds a PGC. in Academic Practice and MA. in Higher Education. Dr Ekpo is a Senior Lecturer in Electrical & Electronic Engineering; leads the Communication and Space Systems Engineering research team at the Manchester Met University, UK; Chartered Engineer; and Senior Fellow of the Higher Education Academy (UK). He is a member of the Institution of Engineering and Technology, IEEE and the American Institute of Aeronautics and Astronautics.